

Research Article

Parameterization-based trajectory planning for an 8-DOF manipulator with multiple constraints

Ziwu Ren^{*}, Zhongyuan Wang, Xiaohan Liu, Rui Lin^{*}

Robotics and Microsystems Research Center, Soochow University, Suzhou 215131, China

ARTICLE INFO

Article history:

Received 29 August 2024

Revised 14 October 2024

Accepted 31 October 2024

Available online 14 November 2024

Keywords:

8-DOF manipulator

Trajectory planning

Parameterization

Obstacle constraints

Teaching-learning-based optimization

ABSTRACT

A physically feasible, reliable, and safe motion is essential for robot operation. A parameterization-based trajectory planning approach is proposed for an 8-DOF manipulator with multiple constraints. The inverse kinematic solution is obtained through an analytical method, and the trajectory is planned in joint space. As such, the trajectory planning of the 8-DOF manipulator is transformed into a parameterization-based trajectory optimization problem within its physical, obstacle and task constraints, and the optimization variables are significantly reduced. Then teaching-learning-based optimization (TLBO) algorithm is employed to search for the redundant parameters to generate an optimal trajectory. Simulation and physical experiment results demonstrate that this approach can effectively solve the trajectory planning problem of the manipulator. Moreover, the planned trajectory has no theoretical end-effector deviation for the task constraint. This approach can provide a reference for the motion planning of other redundant manipulators.

© 2024 The Author(s). Published by Elsevier B.V. on behalf of Shandong University. This is an open access article under the CC BY-NC-ND license (<http://creativecommons.org/licenses/by-nc-nd/4.0/>).

1. Introduction

As a higher organism that has evolved in nature for millions of years, human possesses joint structures that adapt to the complex operation environment. The 8-DOF redundant manipulator simulating the joint of the waist, shoulder, elbow and wrist part of the human being has a model which is similar to the physiological features of the human arm, so it has many functional advantages, such as obstacle avoidance [1,2], singularity avoidance [3,4], larger workspace, more flexible operation [5], etc. For the robotic manipulator, it has been widely applied in typical applications, including object moving [6], milling operation [7], tag labeling, item taking and so on [6,8]. Since the 8-DOF manipulator has more degrees of freedom (DOFs), it is desirable for this robot to perform tasks in a more complex environment.

Theoretically, when executing the motion for a task, there exist infinite configurations that can meet the task constraints for the redundant manipulator. However, besides the task requirements, the manipulator should also satisfy simultaneously the physical constraints [9,10] and the obstacle constraints [11] during the motion. In order to address these various constraints problem, many scholars have presented some methods. Chan and Dubey [9] presented a weighted least-norm solution scheme to solve physical limitations problem for redundant robots. However, this scheme does not guarantee to avoid the obstacle collision. Xiang et al. [12] proposed a general-weighted least-norm

(GWLN) method for the kinematic control of redundant manipulators. Though this method can address the obstacles and joint limits avoidance for the redundant manipulator to a certain extent, it has no capability to avoid the singularity points. Moreover, a tracking error of the trajectory also exists. Wang et al. [13] proposed a novel method to produce an online trajectory for 7-DOF robots with minimum-acceleration planning, where all the kinematic constraints were taken into account from the initial state to the terminal state within a determined time, but this scheme did not take obstacle avoidance into consideration in the workspace. Qi et al. [14] presented an improved A* path planning method based on the inverse kinematics of the 7-DOF space manipulator. However, the search efficiency of the A* algorithm is not very high. Tang et al. [15] presented an obstacle avoidance path planning method based on improved A* algorithm and artificial potential field method. However, the planned trajectory is not very smooth.

The physical limitation, obstacle and task constraints of the robotic manipulator should be effectively addressed to guarantee its safety and reliability of the operation [16]. Since the 8-DOF manipulator has infinite configurations that can meet the task requirement, its trajectory planning will inevitably involve an optimization process. As such, it is essential to formulate the redundancy resolution problem as a constrained optimization problem [17,18]. Also, it is important to find an optimal trajectory that meets the various constraints from all the candidate trajectories. A parameterization-based trajectory planning approach in the joint space for an 8-DOF manipulator with multiple constraints is

^{*} Corresponding authors.

E-mail addresses: zwren@suda.edu.cn (Z. Ren), linrui@suda.edu.cn (R. Lin).

presented in the paper. In this approach, the relevant elements of the optimization problem, i.e., the fitness function, the optimization parameters and the constraint conditions, are formulated. Hence, the trajectory planning of the robot is transformed into a trajectory parameterization optimum problem. Then an evolutionary computation method, that is, teaching-learning-based optimization (TLBO), is employed to search the redundant variables of the trajectory. Simulation results demonstrate the effectiveness of this approach.

Based on the above, the main contributions of this study are highlighted as follows. (1) A parameterization-based trajectory planning method of the 8-DOF manipulator is presented, in which the issue can change into an optimization problem with much fewer variables. Compared with the traditional planning algorithms, this approach can generate trajectory within the physical and obstacle constraints of the robot, and has no theoretical end-effector deviation for the task constraint. (2) This method is applied to a scenario with obstacles, which verifies the superiority of the proposed trajectory planning method.

2. Problem formulation

As shown in Fig. 1, the physical platform of the 8-DOF manipulator is given, where each joint is actuated by the Maxon motor, and the Copley servo driver. All the servo drivers are controlled by a host industrial computer via CAN bus. Distributed control system (DCS) is adopted to realize coordinated multi-axis control. Consider the robot in Fig. 1, Fig. 2 illustrates the corresponding Solidworks model (left) and each joint's axial vector diagram (right). This manipulator imitates the waist, shoulder, elbow and wrist joints structure of the human body, including: (1) a waist joint rotating around the vertical axis upward; (2) three shoulder joints which respectively rotate around the horizontal axis toward left, the horizontal axis toward forward and the vertical axis upward; (3) an elbow joint rotating around the horizontal axis toward forward; (4) three wrist joints that respectively rotate around the vertical axis upward, the horizontal axis toward forward and the horizontal axis toward left.

With reference to the 8-DOF manipulator system, the motion trajectory can be described by the change relationship $\mathbf{q}(t)$ between the joint position vector \mathbf{q} and the time t in the joint space. Then, the $\dot{\mathbf{q}}(t)$ and $\ddot{\mathbf{q}}(t)$ respectively represent the joint speed and acceleration trajectory. Suppose the joint angle vector of the initial point is given by $\mathbf{q}_0 = [q_{00}, q_{10}, q_{20}, \dots, q_{70}]$, the joint angle vector of the point at the terminal moment t_f is represented as $\mathbf{q}_f = [q_{0f}, q_{1f}, q_{2f}, \dots, q_{7f}]$, the joint speed vector and acceleration vector at the initial moment and terminal moment are all $\dot{\mathbf{q}}_0 = \dot{\mathbf{q}}_f = \ddot{\mathbf{q}}_0 = \ddot{\mathbf{q}}_f = \mathbf{0}$, and the position state of the initial point \mathbf{q}_0 is assumed to be known. Then the trajectory planning of the manipulator can be transformed into a parameterization optimization problem, which could be described by the following mathematical model:

$$\mathbf{q}^*(t) = \arg \min f(\mathbf{q}(t)) \quad (1)$$

subject to

$$\begin{aligned} \mathbf{q}^*(0) &= \mathbf{q}_0, & \dot{\mathbf{q}}^*(0) &= \mathbf{0}, & \ddot{\mathbf{q}}^*(0) &= \mathbf{0} \\ \mathbf{q}^*(t_f) &= \mathbf{q}_f, & \dot{\mathbf{q}}^*(t_f) &= \mathbf{0}, & \ddot{\mathbf{q}}^*(t_f) &= \mathbf{0} \end{aligned} \quad (2)$$

where $f(\mathbf{q}(t))$ is a predefined fitness function. Moreover, the motion of the robot is limited by the joint mechanical limits

$$\mathbf{q}_{\min} \leq \mathbf{q}^*(t) \leq \mathbf{q}_{\max}, \quad \forall t \in [0, t_f] \quad (3)$$

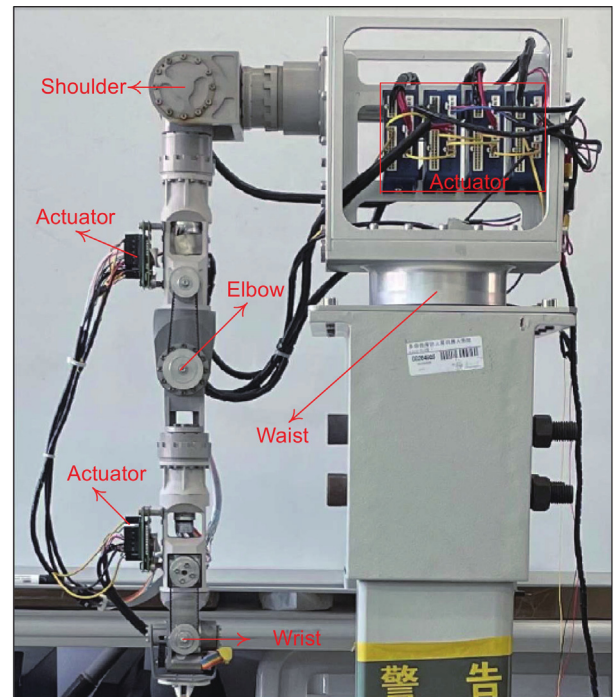


Fig. 1. Actual physical platform of the 8-DOF manipulator.

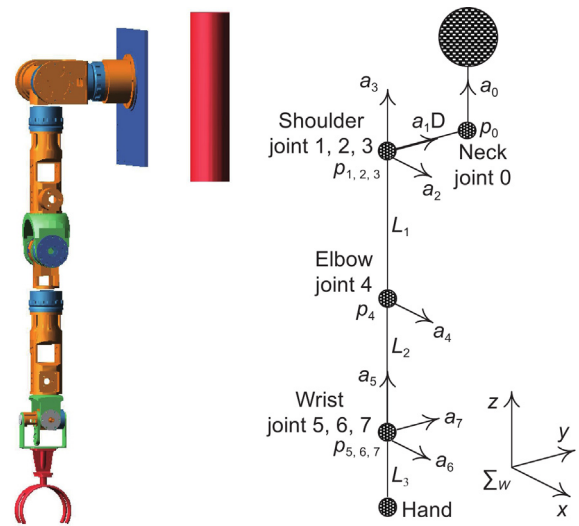


Fig. 2. Solidworks model (left) and each joint's axial vector diagram (right) of the 8-DOF robotic manipulator.

where \mathbf{q}_{\min} and \mathbf{q}_{\max} are the joint mechanical limits, and the joint speeds along the joint trajectory are limited

$$-\dot{\mathbf{q}}_{\max} \leq \dot{\mathbf{q}}^*(t) \leq \dot{\mathbf{q}}_{\max}, \quad \forall t \in [0, t_f] \quad (4)$$

where $\dot{\mathbf{q}}_{\max}$ are the joint speed limits.

Besides the physical constraints of the robot, the obstacle constraints of the manipulator should also be considered, that is, the robot should not collide with obstacles in the workspace during its motion process. As such, several crucial detection points are set on the linkage of the robot and robotic hand, then collision avoidance can be treated as the constraint [17]

$$\mathbf{G}_j(\mathbf{q}^*(t)) \cap \mathbf{S} = \emptyset, \quad \forall t \in [0, t_f] \quad (5)$$

$$j = 1, 2, \dots, s$$

where s is the number of the crucial detection points, \mathbf{S} is the obstacle region defined in the workspace, and $\mathbf{G}_j(\mathbf{q}(t))$ denotes a function that returns the trajectory of the crucial detection point j through the forward kinematics model in the Cartesian coordinate system.

In summary, the Eqs. (1)–(5) constitute the mathematical model of the motion planning of the robot, satisfying the various constraints as well as minimizing the fitness function.

3. Trajectory parameterization of the 8-DOF manipulator

Because of the manipulator redundancy, there are infinite joint trajectories that satisfied the requirements in most cases. As such, the trajectory parameterization process should be performed firstly.

3.1. Forward kinematics analysis

Consider the Solidworks model (left) and each joint's axial vector diagram (right) of the 8-DOF manipulator shown in Fig. 2, where \mathbf{a}_0 is the rotation direction of waist joint, \mathbf{a}_1 – \mathbf{a}_7 are respectively the rotation directions of the shoulder, elbow, and wrist joints, Σ_w is the world coordinate system, D is the shoulder breadth, L_1 is the length of the upper arm, L_2 is the length of the lower arm, and L_3 is the length from the wrist center to the hand center. From Fig. 2, it is obviously seen that the unit vectors of the axes directions \mathbf{a}_0 – \mathbf{a}_7 can be respectively denoted as follows:

$$\begin{cases} \mathbf{a}_0 = (0, 0, 1) & \mathbf{a}_1 = (0, 1, 0) \\ \mathbf{a}_2 = (1, 0, 0) & \mathbf{a}_3 = (0, 0, 1) \\ \mathbf{a}_4 = (1, 0, 0) & \mathbf{a}_5 = (0, 0, 1) \\ \mathbf{a}_6 = (1, 0, 0) & \mathbf{a}_7 = (0, 1, 0) \end{cases} \quad (6)$$

Define the position vector of the robot as $\mathbf{q} = (q_0, q_1, q_2, q_3, q_4, q_5, q_6, q_7)^T$, and the position and orientation of the body(or the neck) are $(\mathbf{p}_0, \mathbf{R}_0)$, where \mathbf{R}_0 is the orientation matrix. Then the position and orientation $(\mathbf{p}_j, \mathbf{R}_j)$ of each connecting rod is [19,20]

$$\begin{cases} \mathbf{p}_j = \mathbf{p}_i + \mathbf{R}_i \mathbf{b}_j \\ \mathbf{R}_j = \mathbf{R}_i \mathbf{R}_{a_j}(q_j) \end{cases} \quad (7)$$

where \mathbf{p}_i is the absolute position coordinate and \mathbf{R}_i is the orientation matrix of the mother linkage in world coordinate system, \mathbf{a}_j is the rotation axis's unit vector and \mathbf{b}_j is the origin coordinate in the coordinate system of the mother linkage, and $\mathbf{R}_{a_j}(q_j)$ is a result that returns the rotation matrix computed by the Rodrigues formula [20] when the joint j rotates q_j radians around its axis vector \mathbf{a}_j . The origin coordinate \mathbf{b}_j ($j = 1, 2, \dots, 8$) in the coordinate system of the mother linkage can be determined as

$$\begin{cases} \mathbf{b}_1 = (0, -D, 0)^T & \mathbf{b}_2 = (0, 0, 0)^T \\ \mathbf{b}_3 = (0, 0, 0)^T & \mathbf{b}_4 = (0, 0, -L_1)^T \\ \mathbf{b}_5 = (0, 0, -L_2)^T & \mathbf{b}_6 = (0, 0, 0)^T \\ \mathbf{b}_7 = (0, 0, 0)^T & \mathbf{b}_8 = (0, 0, -L_3)^T \end{cases} \quad (8)$$

3.2. Analytical inverse kinematics solution

For the 8-DOF redundant robot shown in Fig. 2, there are infinite inverse kinematics solutions because there exist two redundant joints for a certain position and orientation of the end-effector [16,21]. If the waist joint q_0 is zero, then the body orientation \mathbf{R}_0 would be equal to the unit matrix \mathbf{E} . Otherwise, the body orientation is $\mathbf{R}_0 = \mathbf{R}_{a_0}(q_0)$. Since the waist joint is independent of the 7-DOF humanoid arm to some extent, it can be considered as one of the redundant joints for the robot. In addition, there is another redundant joint left on the 7-DOF humanoid arm. Assume that the two redundant joints are adopted

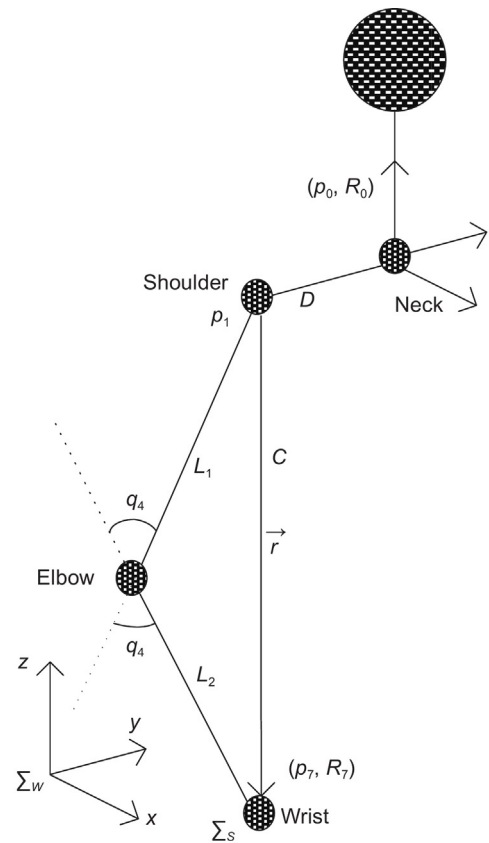


Fig. 3. Elbow joint calculation diagram.

to depict the redundancy of the robot, and the end-effector's desired position and orientation are described by $(\mathbf{p}_7, \mathbf{R}_7)$, \mathbf{p}_7 and \mathbf{R}_7 can be calculated from the formula (28), then how to deal with the inverse kinematics problem of this manipulator quickly and accurately should be solved firstly.

First, compute the position solution of the elbow joint. Fig. 3 is the calculation diagram of the elbow joint position, where the shoulder, elbow and wrist center constitute a triangle. Then the solution of the elbow joint angle q_4 can be directly given by

$$q_4 = \pi - \arccos\left(\frac{L_1^2 + L_2^2 - C^2}{2L_1 \cdot L_2}\right) \quad (9)$$

where L_1 is the length of the upper arm, L_2 is the length of the lower arm, and $C = \|\mathbf{r}\| = \sqrt{r_x^2 + r_y^2 + r_z^2}$ is the length of the vector \mathbf{r} , that is, a directed line from the shoulder center to the wrist center in the body coordinate system, which can be determined by

$$\begin{cases} \mathbf{p}_1 = \mathbf{p}_0 + \mathbf{R}_0 \mathbf{b}_1 \\ \mathbf{r} = \mathbf{R}_0^T (\mathbf{p}_7 - \mathbf{p}_1) = (r_x, r_y, r_z)^T \end{cases} \quad (10)$$

Next, calculate the position solution of the shoulder joints. Fig. 4 is the position calculation diagram of the shoulder joints. When the shoulder joints q_i ($i = 1, 2, 3$) are all equal to 0, the plane constituted by the shoulder, elbow, and the wrist center would be the yoz plane of the body coordinate system. If the shoulder joints rotate q_1, q_2 and q_3 around their respective axis directions, the following equation would be satisfied

$$\mathbf{R}_{a_1}(q_1) \mathbf{R}_{a_2}(q_2) \mathbf{R}_{a_3}(q_3) \begin{pmatrix} 0 \\ y_1 \\ z_1 \end{pmatrix} = \begin{pmatrix} r_x \\ r_y \\ r_z \end{pmatrix} \quad (11)$$

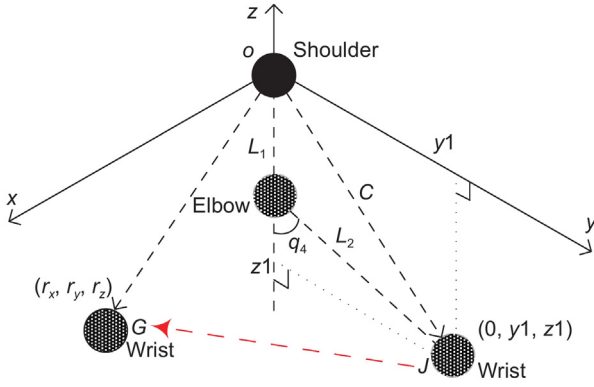


Fig. 4. Shoulder joints calculation diagram.

where $y_1 = L_2 \cdot \sin q_4$ and $z_1 = -\sqrt{C^2 - (L_2 \cdot \sin q_4)^2}$ are the components of the vector \mathbf{r} on the yo_3 plane of the body coordinate system. If the angle q_3 is supposed to be known, then the results of the joints q_1 and q_2 can be given by

$$q_1 = \text{atan2}(-r_z, r_x) \pm \text{atan2}\left(\sqrt{r_x^2 + r_z^2 - (y_1 s_3)^2}, -y_1 s_3\right) \quad (12)$$

$$q_2 = \text{atan2}(-z_1, y_1 c_3) \pm \text{atan2}\left(\sqrt{(y_1 c_3)^2 + z_1^2 - r_y^2}, r_y\right) \quad (13)$$

where the angle abbreviations s_3, c_3 are equal to $s_3 = \sin(q_3)$, $c_3 = \cos(q_3)$ respectively.

Finally, determine the position solution of the wrist joints. Because the rotation matrix relations between the linkages satisfy the formula

$$\mathbf{R}_{a_5}(q_5)\mathbf{R}_{a_6}(q_6)\mathbf{R}_{a_7}(q_7) = \mathbf{R}_{a_4}^{-1}(q_4)\mathbf{R}_{a_3}^{-1}(q_3)\mathbf{R}_{a_2}^{-1}(q_2)\mathbf{R}_{a_1}^{-1}(q_1)\mathbf{R}_{a_0}^{-1}(q_0)\mathbf{R}_7 \quad (14)$$

then the solutions for q_5, q_6 and q_7 can be computed by

$$q_5 = \text{atan2}(-R_{12}, R_{22}) \quad (15)$$

$$q_6 = \text{atan2}(R_{32}, -R_{12}c_5 + R_{22}c_5) \quad (16)$$

$$q_7 = \text{atan2}(-R_{31}, R_{33}) \quad (17)$$

where the abbreviations $s_i = \sin(q_i)$, $c_i = \cos(q_i)$ ($i = 5, 6, 7$), and the R_{ij} ($i = 1, 2, 3$) are the elements of the matrix which can be obtained by

$$\begin{pmatrix} R_{11} & R_{12} & R_{13} \\ R_{21} & R_{22} & R_{23} \\ R_{31} & R_{32} & R_{33} \end{pmatrix} = \mathbf{R}_{a_4}^{-1}(q_4)\mathbf{R}_{a_3}^{-1}(q_3)\mathbf{R}_{a_2}^{-1}(q_2)\mathbf{R}_{a_1}^{-1}(q_1)\mathbf{R}_{a_0}^{-1}(q_0)\mathbf{R}_7 \quad (18)$$

where q_i ($i = 1, 2, 4$) can be derived from the formulas (9), (12) and (13), and the unit vectors $\mathbf{a}_0 \sim \mathbf{a}_4$ are shown in (6).

In brief, the above inverse kinematics solutions are based on the given joints q_0 and q_3 . When given the waist joint angle q_0 and the shoulder joint q_3 , all other joint angles can be derived. The angles q_0 and q_3 can be set as the redundant variables to describe the redundancy of the manipulator.

As formulated above, we plan the motion trajectory of the robot in the joint space. From the boundary conditions shown in (2), that is, the conditions of the joint position meet $\mathbf{q}(0) = \mathbf{q}_0$, $\mathbf{q}(t_f) = \mathbf{q}_f$, the conditions of the joint speed meet $\dot{\mathbf{q}}(0) = \mathbf{0}$, $\dot{\mathbf{q}}(t_f) = \mathbf{0}$, and the conditions of the joint acceleration meet $\ddot{\mathbf{q}}(0) = \mathbf{0}$, $\ddot{\mathbf{q}}(t_f) = \mathbf{0}$, a quintic polynomial strategy can be adopted to interpolate the trajectory of each joint, the quintic polynomial interpolation generates a smooth and continuous trajectory between the initial and final configurations, ensuring that the joint angles q_0 and q_3 vary smoothly over time without abrupt changes.

Thus, there are two parameters that need to be determined during the trajectory parameterization process, that is, q_0 and q_3 , where q_0 is the waist joint position at moment t_f , and q_3 is the redundant joint position of the robot at moment t_f . In brief, the trajectory parameterization of this manipulator can be denoted as $\lambda = (q_0, q_3)$. In order to make the trajectory flexibly operate and satisfy various constraints, we should employ an efficient optimization method to determine these parameters.

4. Trajectory optimization based on teaching-learning-based optimization (TLBO)

Teaching-learning-based optimization (TLBO) [22,23] algorithm is a population-based method inspired from the philosophy of teaching and learning. TLBO algorithm realizes performance improvement through two learning modes, that is, teacher phase and learner phase. In TLBO, the population is comprised of a group of learners, the learner's result is similar to its fitness, and the best solution obtained is deemed as the teacher [24]. Compared with other evolutionary algorithms, TLBO is characterized by a simple concept, few parameter settings, and good computational efficiency. The detailed process of the TLBO is depicted in [22,23].

The redundant manipulator has merits of obstacles avoidance, singularity disposal, manipulability improvement, and so on [25]. Fig. 5 shows different rod configurations of the redundant manipulator for the same target position. From the figure, it can be seen that although there are various link configurations which can reach the same position of the robotic hand center, their manipulability is different from each other. Some configurations are easy to be realized, while others are close to the singularity configuration. In order to make the robot be away from the singularity configuration, the manipulability optimization of the redundant robot at t_f moment is defined as the fitness function of the TLBO. The manipulability of the robot can be defined as a function that is relevant to its Jacobian matrix $\mathbf{J} \in \mathbf{R}^{6 \times 8}$, which is given by [4]

$$\mu = \sqrt{\det(\mathbf{J}\mathbf{J}^T)} \quad (19)$$

where μ is the determinant of the matrix $\mathbf{J}\mathbf{J}^T$. This measure describes the amount of singularity. If the manipulator is singular, the rank of the matrix is not full, resulting in $\mu = 0$. Therefore, a relatively large value μ is beneficial to enhance the manipulability of the manipulator. Hence, the minimized fitness function can be introduced as

$$\min f(\lambda) = \frac{1}{\mu} = \frac{1}{\sqrt{\det(\mathbf{J}\mathbf{J}^T)}} \quad (20)$$

where $\lambda = (q_0, q_3)$ denotes the individual of the TLBO algorithm. The smaller the fitness value, the lower the singularity possibility, which can represent the extent away from the singularity configuration.

Following is the detection whether the selected trajectory $\mathbf{q}(t)$ meets the kinematic constraints (3)–(4) and the obstacles condition (5) or not. If the candidate trajectory $\mathbf{q}(t)$ does not satisfy these constraint conditions, that is

$$\begin{aligned} \mathbf{q}(t) \notin [\mathbf{q}_{\min}, \mathbf{q}_{\max}] \quad \text{or} \quad \dot{\mathbf{q}}(t) \notin [-\dot{\mathbf{q}}_{\max}, \dot{\mathbf{q}}_{\max}] \\ \text{or} \quad \mathbf{G}_j(\mathbf{q}(t)) \cap \mathbf{S} \neq \emptyset, \quad \forall t \in [0, t_f], \quad j = 1, 2, \dots, s \end{aligned} \quad (21)$$

a penalty mechanism is used to punish the fitness function value as follows:

$$\min f(\lambda) = C, \quad C > 0 \quad (22)$$

where C is a penalty parameter which usually is a large positive coefficient, and the meanings of other symbols are the same as in (3)–(5).

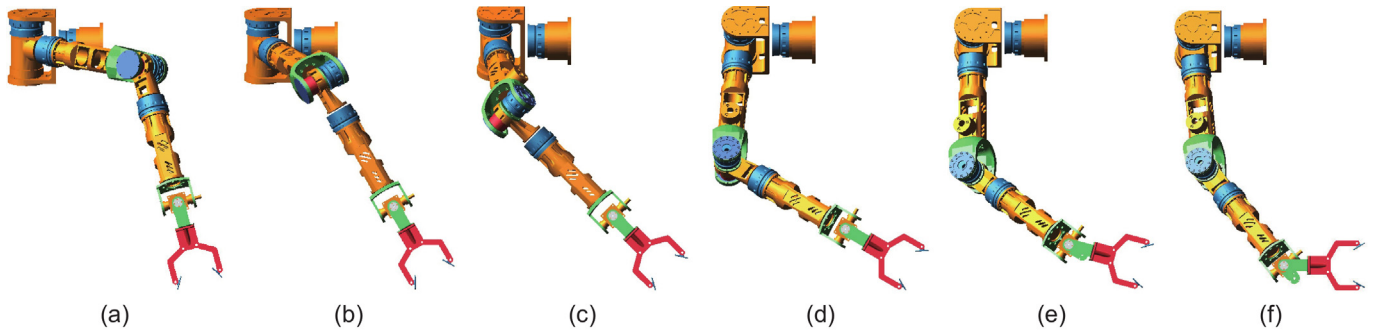


Fig. 5. Different configurations of redundant manipulator for the same target position.

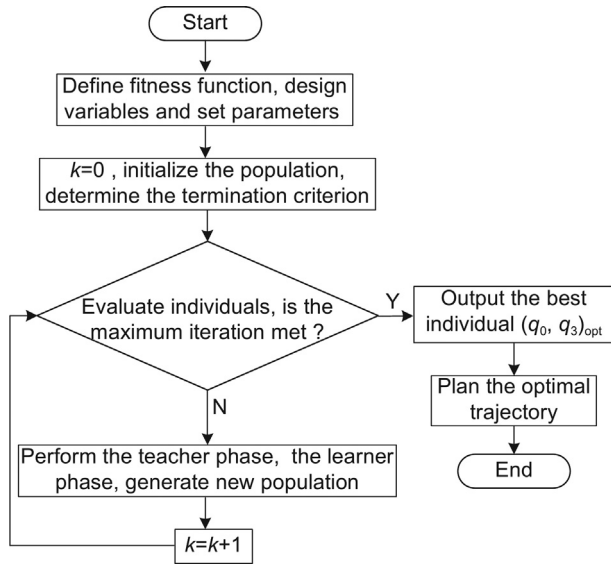


Fig. 6. Optimal trajectory selection of 8-DOF manipulator based on TLBO.

The 8-DOF manipulator has different rod configurations and motion trajectories for the same target task, so we should use an efficient optimization algorithm to select an optimal decision vector according to the defined fitness function. TLBO algorithm is an appropriate method that searches for an optimal solution in multi-dimensional space through the teacher and the learner phase. Based on this, an optimal decision vector $\lambda = (q_0, q_3)$ of the trajectory is determined by the TLBO to minimize the fitness function value without violating various constraints. The optimization primarily focuses on the steady-state part of the trajectory, ensuring that the system reaches the desired final configuration while satisfying the necessary constraints. The procedure of selecting the optimal trajectory based on the TLBO is presented in Fig. 6.

5. Simulation and physical experiments

In order to demonstrate the mechanical performance, the 8-DOF manipulator is firstly compared with the 7-DOF manipulator without the waist joint to manifest its superiority in the aspect of mechanism. Besides this, to demonstrate the planning merits of the presented approach, a simulation scenario with obstacles is established and some simulation and experiments are performed.

Consider the joints' axial vector diagram of the 8-DOF robot shown in Fig. 2, where the origin of the world-coordinate system \sum_w is set at the shoulder center, and the orientation of the body is an identity matrix, that is, $R_0 = E$. In addition,

Table 1

Joint angle range of the 8-DOF manipulator (°).

Range	q_0	q_1	q_2	q_3	q_4	q_5	q_6	q_7
Lower	-30	-126	-133	-180	0	-180	-80	-42
Upper	30	90	15	90	120	180	80	85

Table 2

Maximum joint speed of the 8-DOF manipulator (rad/s).

Joint	\dot{q}_0	\dot{q}_1	\dot{q}_2	\dot{q}_3	\dot{q}_4	\dot{q}_5	\dot{q}_6	\dot{q}_7
Speed	8	13	18	12	20	11	10	4.5

according to the mechanism designed for this manipulator, the corresponding parameters are as follows: the shoulder width is $D = 0.26$ m, the length from the shoulder center to the elbow center is $L_1 = 0.26$ m, the length from the elbow center to the wrist center is $L_2 = 0.26$ m and the length from the wrist center to the hand (clamp) center is $L_3 = 0.14$ m. According to the actual physical and mechanical model in Fig. 1, the permissible range and the maximum speed of each joint are respectively given in Tables 1 and 2.

5.1. Comparison of mechanism performance

To highlight the mechanical merit of the 8-DOF manipulator, the 7-DOF manipulator without the waist joint is added in the experiment, and two comparison experiments were conducted.

As shown in Fig. 7, if the position and orientation (3 Euler angles) of the hand (clamp) center are set as $[0.55 \ 0.25 \ -0.20]$ m, and the orientation is represented by the rotation matrix $R = R_z(\pi/4)R_y(-\pi/2)R_x(0)$, for the 7-DOF manipulator (left), due to the fact that the waist joint position is equal to zero and the target point is relatively far away from the origin of the world-coordinate system, the configuration of the 7-DOF manipulator is almost in a singularity state. On the contrary, because the waist joint can extend the motion range of the manipulator ($q_0 \neq 0$), the 8-DOF manipulator (right) is in a comfortable configuration and retains a certain degree of operability.

As shown in Fig. 8, when the position and orientation (3 Euler angles) of the hand (clamp) center are set to $[0.50 \ 0.35 \ -0.20]$ m, and the orientation is represented by the rotation matrix $R = R_z(-\pi/4)R_y(-\pi/2)R_x(\pi/2)$, the second joint angle of the 7-DOF manipulator (left) reaches its joint limit, making it unable to complete the task due to the waist joint being fixed at zero and the target point being relatively far from the origin of the world-coordinate system. In contrast, the 8-DOF manipulator (right), with its extended motion range from the waist joint ($q_0 \neq 0$), successfully performed the grasping task.

Due to the existence of the waist joint, the 8-DOF manipulator simulates the joint structure of human body, which can further widen its working space, and effectively demonstrate the superiority of its mechanism.



Fig. 7. Configuration comparison of the 7-DOF manipulator without waist joint (left) and the 8-DOF manipulator with waist joint (right).

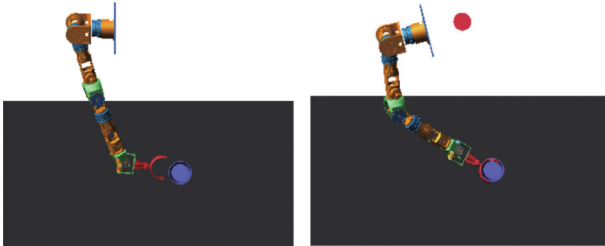


Fig. 8. Configuration comparison of the 7-DOF manipulator without waist joint (left) and the 8-DOF manipulator with waist joint (right).

5.2. Parameterization-based trajectory planning

5.2.1. Parameters of system model

A simulation scenario with obstacles of this 8-DOF manipulator's motion planning is established, as shown in Fig. 9, where the standing cuboid is a static obstacle, and the robot is required to safely move to grab the cup from the static initial point. In this figure, the length, width and height of the cuboid are respectively 0.05 m, 0.05 m and 0.12 m. In this scenario, we set the shoulder center as the origin of the world-coordinate system \sum_w , so the cuboid region \mathcal{S} can be described as

$$\mathcal{S} = \{(x, y, z) \mid 0.27 \leq x \leq 0.32, 0.135 \leq y \leq 0.185, -0.40 \leq z \leq -0.28\} \text{ m} \quad (23)$$

In the experiment, suppose that the position vector of the initial point is determined by

$$\mathbf{q}_0 = [0.0000 \quad 0.4317 \quad -0.5804 \quad -1.1446 \quad 2.0166 \quad 1.5708 \quad 0.9466 \quad -0.3530] \text{ rad} \quad (24)$$

The representation of the task space includes six dimensions, that is, three position elements, and three angle elements for orientation with the angle-axis. In light of the forward kinematic analysis, the initial state of the hand (clamp) center in task space can be given by

$$\mathbf{x}(0) = (0.12 \quad 0.14 \quad -0.25 \quad \pi/2 \quad -\pi/2 \quad 0)^T \quad (25)$$

The linkage configuration of the robot at the initial moment from the front view is shown in Fig. 9.

Assume the terminal time is $t_f = 1$ s, and the terminal position of the hand (clamp) center in task space, which can be obtained from the external vision unit, is as follows:

$$\mathbf{p}_8 = (0.30 \quad 0.26 \quad -0.30)^T \text{ m} \quad (26)$$

If the end-effector's hand(clamp) is in a horizontal manner to grab the cup at moment t_f , then the roll angle ϕ and the pitch angle γ of the hand (clamp), which rotate around the x and y

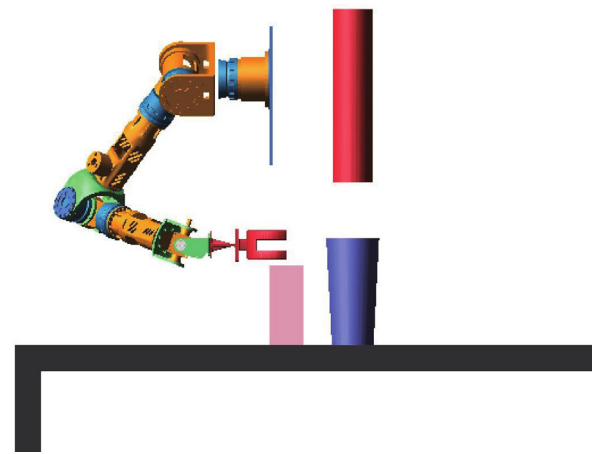


Fig. 9. Front view diagrams of the simulation scenario of the 8-DOF manipulator at the initial moment.

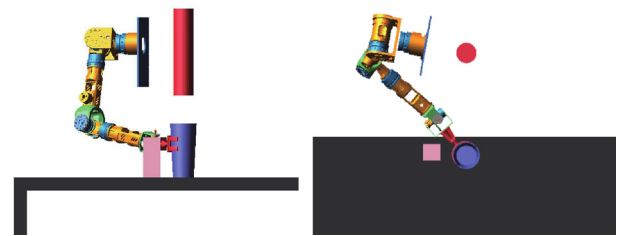


Fig. 10. Configuration diagrams of the simulation scenario of the robot at the terminal moment: front view (left) and vertical view (right).

axis respectively, can be restricted as $\phi = \pi/2$ and $\gamma = -\pi/2$. Thus the orientation of the hand (clamp) can be given by

$$\mathbf{R}_8 = \mathbf{R}_{rpy}(\phi, \gamma, \varphi) = \mathbf{R}_z(\varphi) \mathbf{R}_y(-\pi/2) \mathbf{R}_x(\pi/2) \quad (27)$$

where φ is the yaw angle that rotates around the z axis. Then, when the orientation of the hand (clamp) center is determined, the end-effector's position and orientation ($\mathbf{p}_7, \mathbf{R}_7$) of the 8-DOF robot can be reversely derived by

$$\begin{aligned} \mathbf{R}_7 &= \mathbf{R}_8 \\ \mathbf{p}_7 &= \mathbf{p}_8 - \mathbf{R}_7 \cdot (0 \quad 0 \quad -L_3)^T \end{aligned} \quad (28)$$

From the above, it can be seen that there are three parameters that need to be determined for the motion planning of the manipulator, that is, φ, q_0 and q_3 , where φ is the yaw angle of the clamp's orientation at moment t_f , and q_0 and q_3 are respectively the waist joint position and the redundant joint position of the robot at moment t_f . Hence, the parameters that need to be determined, that is, the decision vector of the trajectory planning of the robot in this scenario can be represented as $(\varphi, \lambda) = (\varphi, q_0, q_3)$.

The goal of the manipulator is to bypass the obstacles and drive its hand (clamp) center to grab the cup. Hereonto, eight crucial points are marked on the hand (clamp) to perform the obstacles detection between the robot and the obstacles during the motion. The coordinates of each mark point under the wrist local coordinate system are defined as follows

$$\begin{aligned} \mathbf{s}_1 &= [0.03, 0.03, -0.14] \text{ m}, & \mathbf{s}_2 &= [0.03, -0.03, -0.14] \text{ m}, \\ \mathbf{s}_3 &= [-0.03, 0.03, -0.14] \text{ m}, & \mathbf{s}_4 &= [-0.03, -0.03, -0.14] \text{ m}, \\ \mathbf{s}_5 &= [-0.011, -0.042, -0.044] \text{ m}, \\ \mathbf{s}_6 &= [0.011, -0.042, -0.044] \text{ m}, \\ \mathbf{s}_7 &= [0.03, 0.03, -0.12] \text{ m}, & \mathbf{s}_8 &= [0.03 - 0.03 - 0.12] \text{ m} \end{aligned} \quad (29)$$

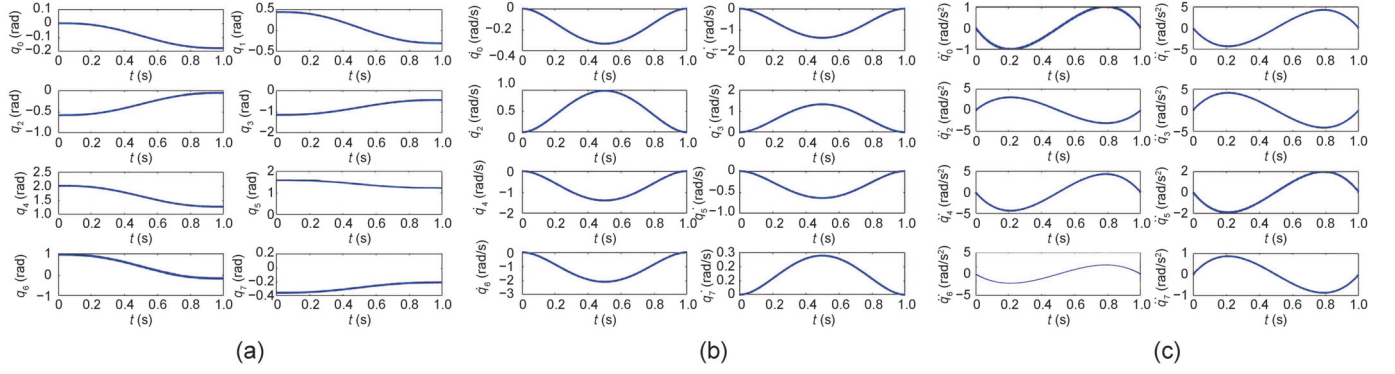


Fig. 11. Position and speed curve of each joint. (a) Position versus time for each joint. (b) Speed versus time for each joint. (c) Acceleration versus time for each joint.

5.2.2. Trajectory planning results

The TLBO-based trajectory optimization of the robot is performed firstly. In TLBO, the evolutionary iteration is set as $G=15$, the population size is $NP=20$, the individual of the TLBO is $(\varphi, \lambda) = (\varphi, q_0, q_3)$, the range limitation of the yaw angle $\varphi \in [-\pi/2, \pi/2]$, and the range limitations of q_0 and q_3 are shown in Table 1, respectively. Moreover, the fitness function of TLBO is formulated as Eqs. (19)–(22). If the selected trajectory violates the kinematic or obstacles constraints, the penalty coefficient $C = 10^6$ is offered to its fitness value. Through iteration optimization, the optimal decision vector can be obtained by

$$(\varphi, q_0, q_3)_{opt} = (-0.8724, -0.1764, -0.4418) \text{ rad} \quad (30)$$

where the corresponding fitness value is 15.7388. According to this result, it can be concluded that the planned trajectory satisfies the kinematic and obstacles constraints of the robot during the motion.

Substituting the obtained result $(\varphi, q_0, q_3)_{opt}$ into the geometric expression of the inverse kinematics, the corresponding solution at moment t_f can be obtained as follows:

$$\mathbf{q}_f = [-0.1764 \quad -0.3039 \quad -0.0578 \quad -0.4418 \quad 1.2768 \quad 1.2314 \quad -0.1663 \quad -0.2055] \text{ rad} \quad (31)$$

The corresponding linkage configuration of the robot at moment t_f is shown in Fig. 10. From the figure, it can be seen that the end-effector's hand(clamp) can accurately reach the desired point and grab the cup in a horizontal manner with a certain yaw angle.

Fig. 11 respectively shows the position, speed, and acceleration curves of each joint for the planned trajectory. In the figure, the whole motion time is 1.0 s. It can be seen that the joint trajectories are sufficiently smooth during the motion process. Moreover, the position, speed, and acceleration trajectories of all joints respectively meet the physical limitations shown in Tables 1 and 2, which indicates that this trajectory can be executed for the robot.

Fig. 12 shows a simple presentation of the robot during the whole motion process in three-dimensional space. Fig. 13 demonstrates the linkage configuration diagrams of the robot every 0.25 s in the simulation scenario from the vertical view. It can be seen that there is no interference between the manipulator and the cuboid obstacle during the motion, and the hand (clamp) can grab the cup successfully. Because this approach obtains the inverse kinematics solution using an analytical method, it has no position and orientation's error in theory when the clamp grabs the cup at moment t_f .

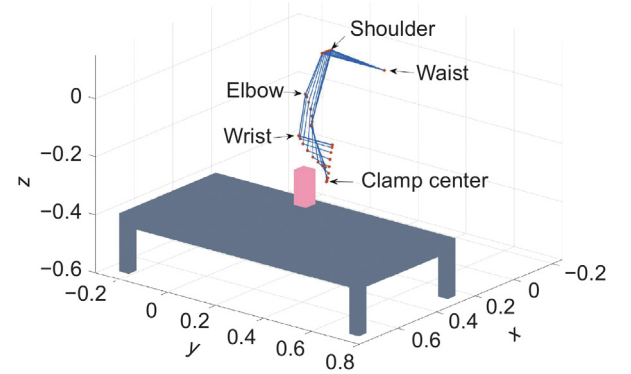


Fig. 12. Simple presentation of the manipulator in 3-D space by the proposed approach.

5.2.3. Comparison with the gradient projection method (GPM)

To validate the effectiveness of the presented approach for the trajectory planning of the 8-DOF manipulator, the traditional gradient projection method (GPM) [26,27] which has been widely employed for the robot's kinematic control, is adopted to plan the trajectory. The joint speed vectors computed by the GPM method are formulated as [26,27]

$$\dot{\mathbf{q}} = \mathbf{J}^+ \dot{\mathbf{x}} + k(\mathbf{I} - \mathbf{J}^+ \mathbf{J}) \nabla H(\mathbf{q})^T \quad (32)$$

where $\dot{\mathbf{x}}$ is a vector which is composed of linear velocity and rotational velocity, $\dot{\mathbf{q}}$ is the joint speeds, \mathbf{J} is the Jacobian matrix, \mathbf{J}^+ is the Moore-Penrose inverse of the Jacobian matrix, k is a real scalar coefficient, and $\nabla H(\mathbf{q})$ is the gradient vector of the criterion that is defined as [9,12]

$$H(\mathbf{q}) = \sum_{i=1}^8 \frac{(q_{i\max} - q_{i\min})^2}{(q_{i\max} - q_i)(q_i - q_{i\min})} \quad (33)$$

where q_i is the i th joint position, and $q_{i\max}$ and $q_{i\min}$ are the upper boundary and lower boundary of the joint q_i , respectively. The goal is to drive the end-effector tool (clamp) to grab the cup. Assume that the clamp's orientation of the terminal moment t_f is the same as that of the initial moment t_0 , then the initial state and terminal state in task space is respectively as follows:

$$\mathbf{x}(0) = (0.12 \quad 0.14 \quad -0.25 \quad \pi/2 \quad -\pi/2 \quad 0)^T \quad (34)$$

$$\mathbf{x}(1) = (0.30 \quad 0.26 \quad -0.30 \quad \pi/2 \quad -\pi/2 \quad 0)^T \quad (35)$$

The trajectory $\mathbf{x}(t)$ of task space is also interpolated by the quintic polynomial strategy.

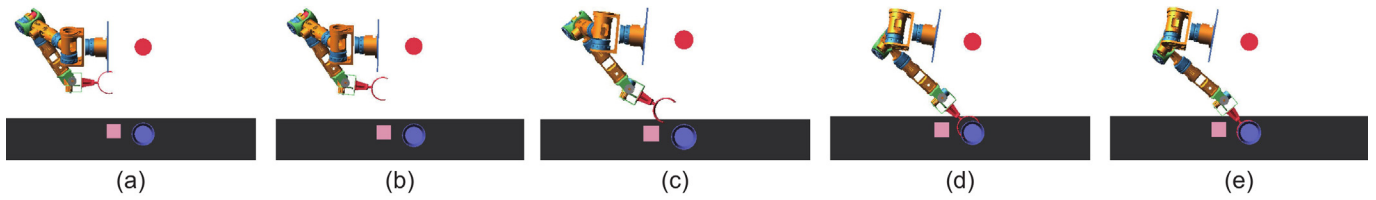


Fig. 13. Linkage configurations change of the 8-DOF manipulator from the vertical view for the planned trajectory. (a) $t=0.0$ s. (b) $t=0.25$ s. (c) $t=0.50$ s. (d) $t=0.75$ s. (e) $t=1.0$ s.

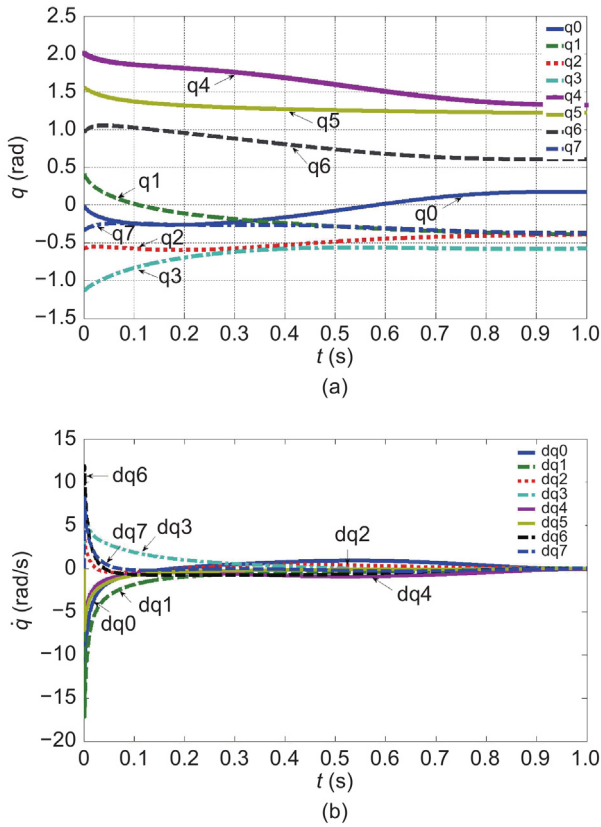


Fig. 14. Trajectories of joint positions and speeds by the GPM method. (a) Position versus time for each joint. (b) Speed versus time for each joint.

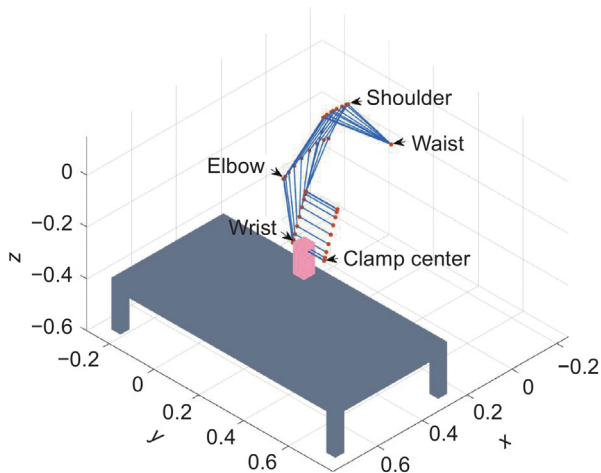


Fig. 15. Simple presentation of the manipulator in 3-D space by the GPM method.

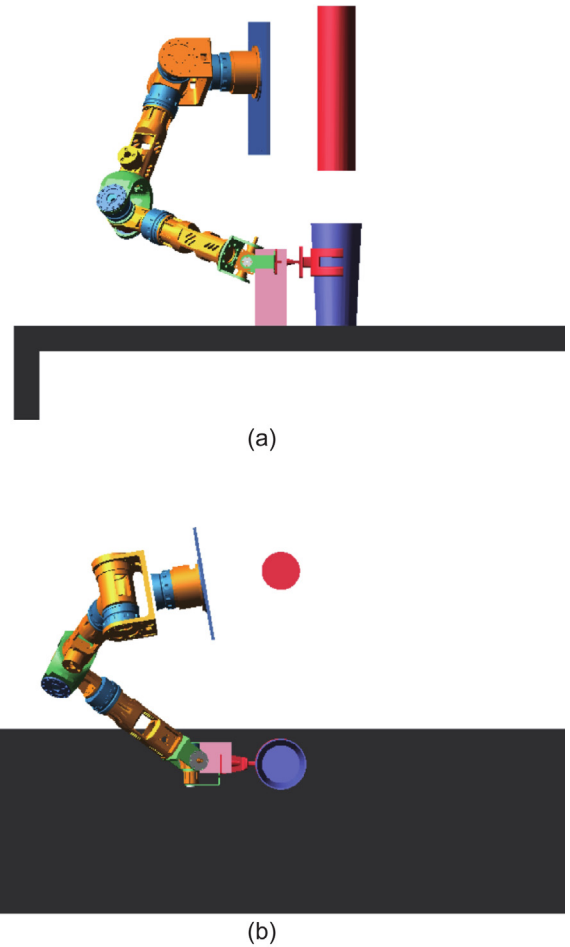


Fig. 16. Linkage configurations at the terminal moment of the robot by the GPM method. (a) Configuration diagram from the front view. (b) Configuration diagram from the vertical view.

Fig. 14 shows the planned trajectories of the joint positions and speeds by the GPM method. The maximum speed values of the joints are respectively given by

$$\dot{q}_{max} = [12.3788 \quad 17.1667 \quad 3.7111 \quad 7.8287 \quad 6.3326 \quad 7.1530 \quad 11.9435 \quad 8.2137] \text{ rad/s} \quad (36)$$

It can be seen that several maximum joint speeds, for example, \dot{q}_0 , \dot{q}_1 , \dot{q}_6 and \dot{q}_7 , have violated the corresponding joint speed constraints shown in Table 2, which would give rise to low trajectory tracking control accuracy and even harm the actuators of the robot [28]. Fig. 15 demonstrates the simplified presentation of the 8-DOF manipulator in 3-D space by the GPM method, in which it can be seen that the axis line between the wrist and the hand (clamp) center has entered the area of the obstacle at moment t_f . Fig. 16 shows the linkage configurations at the

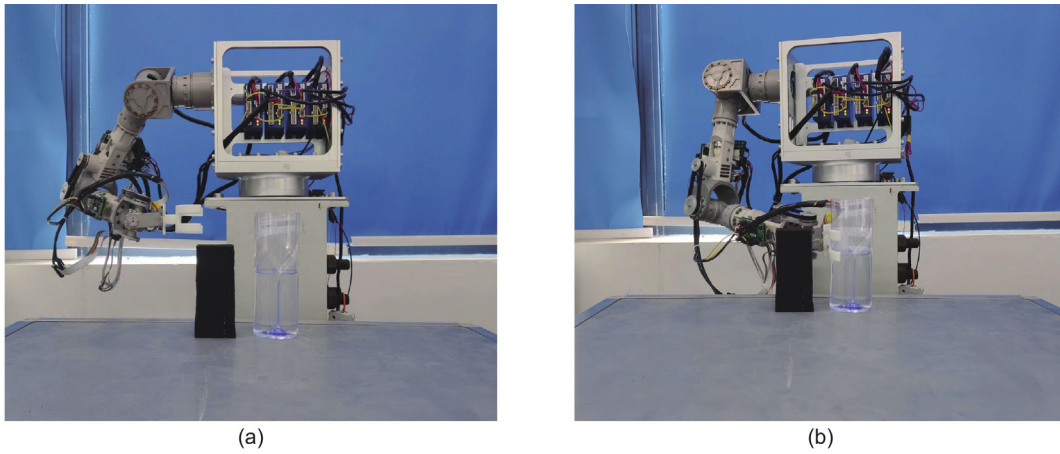


Fig. 17. Front view diagrams of the robotic platform at the initial and terminal moment. (a) Front view diagrams at initial moment. (b) Front view diagrams at terminal moment.

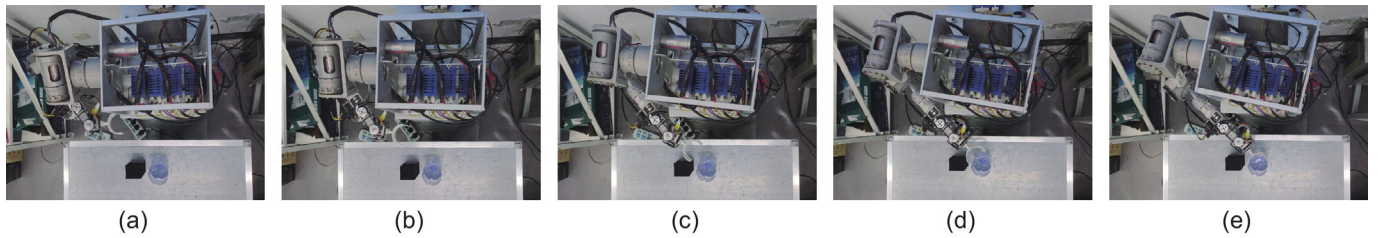


Fig. 18. Linkage configurations change of the robotic platform from the vertical view for the planned trajectory. (a) $t=0.0$ s. (b) $t=0.25$ s. (c) $t=0.50$ s. (d) $t=0.75$ s. (e) $t=1.0$ s.

Table 3
Comparison results of different trajectory planning methods.

Methods	Variable dimensions	$err(\Delta\mathbf{p}, \Delta\mathbf{R})$	t/s	$f(\lambda)$
Gradient Projection Method ^a	8	$9.9216e-7$	0.0923	15.0810
Proposed approach	3	0	0.0256	14.9387

^a In the GPM, the clamp's orientation of the terminal moment t_f is the same as that of the initial moment t_0 , that is, the yaw angle $\varphi = 0$ of the clamp at moment t_f .

terminal moment in the simulation scenario from the front and vertical view, where it can also be found that the position and orientation of the hand (clamp) are basically in accord with the terminal state in task space shown in (35), but the connectors of the wrist have interfered with the obstacle severely and the selected trajectory does not meet the obstacle constraints. The GPM method plans the trajectory of the manipulator in task space through the iteration, so it exists cumulative error during the iteration process. Moreover, the scalar coefficient k value of the GPM method in (33) has a great impact on the error accuracy [12].

To further verify the advantages of the proposed approach, the proposed approach is compared with the GPM in terms of running time, and solution accuracy at moment t_f . In GPM, the optimization variable dimensions are 8, the scalar coefficient k is set as 0.86 and the maximum evolutionary iteration of the GPM is $T = 2500$. Once the clamp's position and orientation error at moment t_f , which is defined as $err(\Delta\mathbf{p}, \Delta\mathbf{R})$ [21], is less than 10^{-6} , the whole GPM iteration procedure will stop immediately. Table 3 lists the comparison results between the GPM and the proposed planning approach.

As shown in Table 3, the variable dimensions of the proposed approach in this paper are much smaller than the corresponding value of the GPM. At the same time, the proposed approach also has advantages over the GPM in terms of the clamp's position and orientation error at moment t_f and the running time t . Additionally, the proposed approach demonstrates better operability, with

a lower $f(\lambda)$ value compared to the GPM, which reflects improved efficiency and control in task execution.

In brief, the GPM cannot guarantee to meet the constraint issues due to its local optimal solution. The proposed approach has great advantages compared with the traditional GPM. However, the approach also has certain limitations, in which the analytical inverse kinematics solution of this approach greatly depends on the particular joint model of the robot, and it lacks a certain universality.

5.2.4. Practical testing of the robotic platform

To verify the effectiveness of the proposed approach, the physical experiment is conducted on the robotic platform. The actual physical platform of the 8-DOF manipulator is shown in Fig. 1. The console application is written using Microsoft Visual Studio compiler software, which sends the program instructions to each actuator through the CAN bus to control the motion of the manipulator.

Fig. 17 shows the actual linkage configurations of the robotic platform at the initial (left) and terminal (right) moment. It can be seen that the end-effector's clamp can accurately reach the initial point with the desired position and orientation shown in the formula (25), and grasp the cup in a horizontal manner with a certain yaw angle, where the position and orientation of the clamp center are respectively given by the formula (26), (27) and (30). Fig. 18 shows the linkage configurations change of the

robotic platform's practical testing at different moments. It can also be seen that there is no collision between the manipulator and the obstacle during the whole motion, and the practical linkage configurations at different moments are consistent with the corresponding configurations shown in Fig. 13.

6. Conclusion

In this paper, a parameterization-based trajectory planning approach is presented for the 8-DOF manipulator with multiple constraints. By introducing trajectory parameterization, the number of trajectory variables is significantly reduced, and the resulting trajectory satisfies the physical, obstacle, and task constraints of the manipulator. Moreover, the planned trajectory theoretically shows no end-effector deviation. Simulation and physical experiment results demonstrate the effectiveness of this approach.

Although this method was specifically designed and validated for an 8-DOF redundant manipulator, its core concept is broadly applicable to other degrees of freedom (DOF) robotic systems, such as 7-DOF or 6-DOF manipulators. In a 7-DOF system, while the removal of joint 0 (waist joint) may reduce the workspace, by appropriately adjusting the dimensionality of the optimization variables, the method can still efficiently plan trajectories. Similarly, in a 6-DOF system, this approach can be adapted to achieve effective trajectory planning by adjusting the optimization parameters and task constraints.

Additionally, this approach is also applicable to higher-DOF systems, such as 9-DOF or more. In such systems, the added redundancy provides even more flexibility in task optimization, especially for complex tasks or constrained environments. The increased degrees of freedom allow for more versatile motion planning, and our method can handle this redundancy effectively through careful design of the optimization parameters, ensuring that the trajectory remains accurate and efficient under more complex constraints.

In future work, we plan to conduct further physical experiments to validate this approach across different manipulator configurations, enhancing its applicability and effectiveness for a wide range of redundant manipulator systems.

CRedit authorship contribution statement

Ziwu Ren: Writing – original draft, Investigation, Conceptualization. **Zhongyuan Wang:** Writing – review & editing, Data curation. **Xiaohan Liu:** Writing – review & editing, Validation. **Rui Lin:** Writing – original draft, Supervision, Conceptualization.

Declaration of competing interest

The authors declare that they have no known competing financial interests or personal relationships that could have appeared to influence the work reported in this paper.

Acknowledgments

This work is supported by Jiangsu (Industry Foresight and Key Core Technology) Key Research and Development Project (BE2022137), and the National Natural Science Foundation of China (51675358).

Appendix A. Supplementary data

Supplementary material related to this article can be found online at <https://doi.org/10.1016/j.birob.2024.100193>.

References

- [1] D. Guo, Y. Zhang, Acceleration-level inequality-based MAN scheme for obstacle avoidance of redundant robot manipulators, *IEEE Trans. Ind. Electron.* 61 (12) (2014) 6903–6914.
- [2] A.H. Khan, S. Li, X. Luo, Obstacle avoidance and tracking control of redundant robotic manipulator: An RNN-based metaheuristic approach, *IEEE Trans. Ind. Inform.* 16 (7) (2020) 4670–4680.
- [3] H. Huang, T. Zhang, C. Yang, C.L.P. Chen, Motor learning and generalization using broad learning adaptive neural control, *IEEE Trans. Ind. Electron.* 67 (10) (2020) 8608–8617.
- [4] S. Patel, T. Sobh, Manipulator performance measures – a comprehensive literature survey, *J. Intell. Robot. Syst.* 77 (2015) 547–570.
- [5] G. Song, S. Su, Y. Li, X. Zhao, H. Du, J. Han, Y. Zhao, A closed-loop framework for the inverse kinematics of the 7 degrees of freedom manipulator, *Robotica* 39 (4) (2021) 572–581.
- [6] H. Wang, H. Wang, J. Huang, B. Zhao, L. Quan, Smooth point-to-point trajectory planning for industrial robots with kinematical constraints based on high-order polynomial curve, *Mech. Mach. Theory* 139 (2019) 284–293.
- [7] H.N. Huynh, H. Assadi, E. Rivière-Lorphèvre, O. Verlinden, K. Ahmadi, Modelling the dynamics of industrial robots for milling operations, *Robot. Comput.-Integr. Manuf.* 61 (2020) 101852.
- [8] L. Jin, F. Zhang, M. Liu, S.S.-D. Xu, Finite-time model predictive tracking control of position and orientation for redundant manipulators, *IEEE Trans. Ind. Electron.* 70 (6) (2023) 6017–6026.
- [9] T. Chan, R. Dubey, A weighted least-norm solution based scheme for avoiding joint limits for redundant manipulators, in: [1993] Proceedings IEEE International Conference on Robotics and Automation, vol. 3, 1993, pp. 395–402.
- [10] M. Liu, J. Fan, Y. Zheng, S. Li, L. Jin, A simultaneous learning and control scheme for redundant manipulators with physical constraints on decision variable and its derivative, *IEEE Trans. Ind. Electron.* 69 (10) (2022) 10301–10310.
- [11] Z. Zhang, S. Chen, X. Zhu, Z. Yan, Two hybrid end-effector posture-maintaining and obstacle-limits avoidance schemes for redundant robot manipulators, *IEEE Trans. Ind. Inform.* 16 (2) (2020) 754–763.
- [12] J. Xiang, C. Zhong, W. Wei, General-weighted least-norm control for redundant manipulators, *IEEE Trans. Robot.* 26 (4) (2010) 660–669.
- [13] Y. Wang, L. Sun, L. Zhou, J. Liu, Online minimum-acceleration trajectory planning with the kinematic constraints, *Acta Automat. Sinica* 40 (7) (2014) 1328–1338.
- [14] Z. Qi, P. Huang, Z. Liu, D. Han, Research on path planning method of spatial redundant manipulator, *Acta Automat. Sinica* 45 (6) (2019) 1103–1110.
- [15] X. Tang, H. Zhou, T. Xu, Obstacle avoidance path planning of 6-DOF robotic arm based on improved A* algorithm and artificial potential field method, *Robotica* 42 (2) (2024) 457–481.
- [16] Z. Ren, B. Hu, Z. Wang, L. Sun, Q. Zhu, Knowledge database-based multiobjective trajectory planning of 7-DOF manipulator with rapid and continuous response to uncertain fast-flying objects, *IEEE Trans. Robot.* 39 (2) (2023) 1012–1028.
- [17] Z.W. Ren, Q.G. Zhu, R. Xiong, Trajectory planning of 7-DOF humanoid manipulator under rapid and continuous reaction and obstacle avoidance environment, *Zidonghua Xuebao/Acta Automatica Sinica* 41 (6) (2015) 1131–1144.
- [18] M. Galicki, The planning of robotic optimal motions in the presence of obstacles, *Int. J. Robot. Res.* 17 (3) (1998) 248–259.
- [19] Z. Ren, Z. Wang, Z. Guo, L. Fan, An optimal configuration solution of 8-DOF redundant manipulator for flying ball, in: *Intelligent Robotics and Applications*, Springer Nature Singapore, Singapore, 2023, pp. 476–487.
- [20] S. Kajita, *Humanoid Robots*, Tsinghua University Press, Beijing, China, 2007.
- [21] R. Ziwu, A joint physical constraints avoidance method for inverse kinematics problem of redundant humanoid manipulator, *J. Mech. Eng.* 50 (2014) 58.
- [22] R. Rao, V. Savsani, D. Vakharia, Teaching-learning-based optimization: A novel method for constrained mechanical design optimization problems, *Comput. Aided Des.* 43 (3) (2011) 303–315.
- [23] R. Rao, V. Savsani, D. Vakharia, Teaching-learning-based optimization: An optimization method for continuous non-linear large scale problems, *Inform. Sci.* 183 (1) (2012) 1–15.
- [24] R.V. Rao, V. Patel, An improved teaching-learning-based optimization algorithm for solving unconstrained optimization problems, *Sci. Iran.* 20 (3) (2013) 710–720.
- [25] W. Xu, J. Zhang, B. Liang, B. Li, Singularity analysis and avoidance for robot manipulators with nonspherical wrists, *IEEE Trans. Ind. Electron.* 63 (1) (2016) 277–290.
- [26] R. Dubey, J. Euler, S. Babcock, Real-time implementation of an optimization scheme for seven-degree-of-freedom redundant manipulators, *IEEE Trans. Robot. Autom.* 7 (5) (1991) 579–588.
- [27] Automatic supervisory control of the configuration and behavior of multibody mechanisms, *IEEE Trans. Syst. Man Cybern.* 7 (12) (1977) 868–871.
- [28] D. Chen, Y. Zhang, A hybrid multi-objective scheme applied to redundant robot manipulators, *IEEE Trans. Autom. Sci. Eng.* 14 (3) (2017) 1337–1350.